International Journal of Heat and Mass Transfer 141 (2019) 685–695

Contents lists available at ScienceDirect

International Journal of Heat and Mass Transfer

journal homepage: www.elsevier.com/locate/ijhmt

Multicomponent drop breakup during impact with heated walls

Abhijeet Chausalkar, Song-Charng Kong, James B. Michael *

H.M. Black Engineering, Department of Mechanical Engineering, Iowa State University, Ames, IA 50011, United States

ARTICLE INFO

Article history:
Received 5 March 2019
Received in revised form 25 May 2019
Accepted 10 June 2019

Keywords:
Drop-wall interaction
Leidenfrost effect
Liquid-vapor phase change
Multicomponent fuels

ABSTRACT

Understanding multicomponent drop breakup during impact with walls is critical to the prediction and optimization of fuel-air mixture distribution in combustion systems. In combustors, drops impact walls over a range of wall temperatures and drop velocities, resulting in complex outcomes. In this paper, the regimes of drop impact are characterized for bicomponent and multicomponent fuel drops impacting hot walls. Mixtures of n-heptane and n-decane were used to represent low and high boiling point fuel components, respectively. The wall surface temperatures were varied from 27 to 400 °C with drop Weber numbers ranging up to ~700 for a range of mixing ratios of n-heptane and n-decane. The drop impact events were recorded using high-speed imaging, allowing the identification of impact outcomes and classification into regimes of film deposition, nucleate boiling, and rebound at low Weber numbers, and splashing and breakup at high Weber numbers. In bicomponent mixtures of n-heptane and n-decane, increasing the fraction of the volatile component (n-heptane) results in secondary film breakup at low wall temperatures and a shift in the classified regimes of impact. The droplet size distribution following this secondary breakup was determined, and results show a decrease in the mean droplet size with increasing volatile concentration. Finally, commercial gasoline and diesel fuel drops were examined over similar wall temperature and Weber number ranges. The impact regimes are comparable to those identified for the well-defined bicomponent liquid mixture, in which more volatile components promote rebound and disintegration of the liquid.

1. Introduction

Many industrial spray processes involve small sub-millimeter-scale drops impinging on solid walls. In particular, spray cooling and sprays in combustion systems exhibit liquid drops or sprays interacting with solid surfaces that may be well above the liquid boiling temperature. In both cases, identifying the controlling physical parameters is essential to optimize the heat transfer rate or vaporization duration. In spray cooling, liquid sprays impinge on heated surfaces to facilitate rapid cooling by undergoing phase change. The liquid deposits as a film and the phase change occurs primarily in a nucleate boiling regime [1,2]. The rate of cooling depends on the extent of heat transfer between the wall and drop, and is controlled by the rate of vapor formation near the wall [2]. In combustion sprays, multicomponent fuels such as gasoline or diesel fuel are injected at high pressures to achieve improved fuel economy and lower exhaust emissions [3,4]. These injection pressures result in atomization of the liquid fuel into micrometer-scale droplets and allow for desirable vaporization and mixing for optimal combustion. After injection, droplets span a wide range of velocities and sizes. In certain operating conditions fuel drops can impinge on piston surfaces. These wall temperatures vary periodically because of the changing operating speed and load conditions, adding to the complexity of modeling spray-wall interactions. Variations in wall temperature and the resulting drop-wall interaction can impact overall combustion performance and pollutant emissions [5–7]. For example, increased unburned hydrocarbon emissions have been attributed to the formation of a thin liquid film at the wall [7].

For combustion and spray cooling applications, both the liquid and wall properties control the ultimate outcome of drop-wall interactions. Several dimensionless parameters have been used to characterize the outcomes of drop-wall interactions. A number of studies have examined the influence of the dimensionless Reynolds, Weber, and Ohnesorge numbers on the outcome of a drop impact on the wall [8–10]. The Reynolds number,

$$Re = \frac{\rho_\ell U d_0}{\mu_\ell}, \tag{1}$$

is defined as the ratio of inertial to viscous forces using the liquid density (ρ_ℓ), drop diameter (d_0), liquid viscosity (μ_ℓ), and the

* Corresponding author.
E-mail address: jmichael@iastate.edu (J.B. Michael).

https://doi.org/10.1016/j.ijheatmasstransfer.2019.06.033
0017-9310/

relative velocity at impact (U). The Ohnesorge number, which is the ratio of viscous forces to the combined inertial and surface tension forces is defined as

$$Oh = \frac{\mu_\ell}{\sqrt{\rho_\ell \sigma d_0}}, \tag{2}$$

with σ the liquid-vapor surface tension. From these, another dimensionless parameter, the Weber number, can be formed describing the relative effect of fluid inertia and surface tension:

$$We = Oh \cdot Re^2 = \frac{\rho_\ell U^2 d_0}{\sigma}. \tag{3}$$

These parameters have been used successfully to establish regimes of drop-wall interaction using a critical splashing parameter (K_c) with the form $K_c = OhRe^n$. Various correlations of this form have been proposed by Stow and Hadfield [11], Mundo et al. [12], Cossali et al. [13], and van der Wal [14]. These empirical relations successfully predict the onset of splashing for drops impacting a cold wall, with small droplets produced at the perimeter of the expanding liquid film. In addition, empirical correlations for drop spreading rate have been proposed with both *We* and *Re*. The maximum liquid film spread on cold, dry walls has been shown to increase with increasing drop momentum [15–17]. Correlations were established to quantify the influence of drop diameter, liquid viscosity, and surface tension on the film spreading rate and maximum spread [17]. For the same Weber number but different Reynolds numbers, higher liquid viscosity and smaller drop diameter (low *Re*) were shown to decrease the maximum spread. However, for the same Reynolds number but increased Weber number, the relative increase in surface tension resulted in a reduction in the total spread of the liquid film [17].

During the drop-wall interaction, differences in the drop surface temperature (T_s) and the wall temperature (T_w) have also been shown to result in different outcomes. A number of studies report variations in impact behavior depending on both the hydrodynamic regime and wall temperature [18–20]. These outcomes can be grouped into four regimes based on the wall temperature [9,21,22]:

- Film evaporation ($T_w < T_{sat}$)
- Nucleate boiling ($T_{sat} < T_w < T_{Nukiyama}$)
- Transition boiling ($T_{Nukiyama} < T_w < T_{Leidenfrost}$)
- Film boiling ($T_w > T_{Leidenfrost}$)

Here, the wall temperature (T_w) and the liquid saturation temperature (T_{sat}) are well defined for a pure fluid. For a given liquid and wall substrate, two other temperatures are reported in the literature defining boundaries between the observed regimes: the Leidenfrost temperature, corresponding to the temperature of minimum heat flux for a near-stationary drop ($T_{Leidenfrost}$), and the Nukiyama temperature, corresponding to the maximum heat flux ($T_{Nukiyama}$) [23].

In the case of film evaporation, where the temperature is below the liquid saturation temperature, the drop spreads on the solid surface and forms a thin liquid film which wets the wall. This regime is characterized by slow evaporation of the liquid without the observation of bubble nucleation at the wall. A previous study described the variation in maximum spreading rate and the rate of recoil with wall temperature using n-heptane for a low impact Weber number of 43 [24]. However, this investigation was limited to a single component fuel, and the author recommended the use of high-speed image sequences to capture the fast dynamics of drop spread and rebound in future studies. Similar studies have examined the variation in spread factor for a range of wall temperatures but have focused on single-component liquids at lower Weber numbers [24–26]. In the film evaporation regime (low temperature), the role of fuel composition on the spread and recoil of the liquid film was examined recently [27]. In the study, the spreading of both single and bicomponent fuel drops were comparable, and the vaporization times decreased with increasing wall temperature [27].

As the wall temperature increases to the saturation temperature, a nucleate boiling regime is observed, with bubbling/boiling phenomena beginning shortly after the drop impact. The onset of the nucleate boiling regime is characterized by rapid vapor nucleation and the ejection of small-scale droplets as bubbles emerge from the liquid surface. The wall serves as a site for heterogeneous nucleation, and vapor bubbles formed at the wall-liquid interface dominate the vaporization. As the wall temperature continues to rise, the heat transfer rate to the drop is sufficient to cause vaporization prior to the drop reaching the wall surface. Above a certain temperature, the formation of a vapor layer results in rebound of the drop without direct contact between the liquid and the wall surface, and this is referred to as a film boiling regime. This temperature is defined by a minimum value of the heat flux between the wall and the drop and is referred to as the Leidenfrost temperature ($T_{Leidenfrost}$) [28,29]. For low impact momentum, the drop will rebound without breaking up. At higher impact momentum, breakup may take place, but vapor formation limits direct liquid-wall contact [30].

Between the nucleate-boiling and film-boiling regimes, a transitional regime is observed where evidence of a vapor layer is observed but direct liquid-wall contact still takes place. This period is of interest as the rate of drop heating and morphology of the vaporizing liquid drop vary significantly during the transition. An additional temperature can be used to describe the onset of this transition boiling regime. The Nukiyama temperature ($T_{Nukiyama}$), as previously described, is defined by the minimum time to completely vaporize a low-momentum drop. Few studies report transition regimes for single and bicomponent fuel mixtures; therefore, there is a need to experimentally identify boundaries for both single and bicomponent fuel mixtures.

In addition to high wall temperature, combustion and spray cooling applications may have significant variations in drop velocity at the time of wall impact. As the drop impact velocity varies for cold walls, characteristic outcomes range from deposition without splashing to deposition with splashing. The outcomes have been summarized with regime diagrams by showing a *Oh* and *Re* boundary between non-splashing and splashing outcomes. At elevated wall temperature, the majority of prior studies have focused on low and moderate momentum drops impacting hot walls. A number of studies have comprehensively identified disintegration limits for drops on hot walls for a number of pure components [30–32]. In addition, the surface roughness amplitude has been shown to decrease the disintegration of drops and generation of secondary droplets. Increased roughness generates fewer secondary droplets, which is attributed to vapor formation in surface roughness voids/-valleys [31]. Moita et al. correlated secondary droplet size with the Sauter mean diameter, Weber number, and Reynolds number in the film boiling regime [32]. However, the correlations established were only valid for surface roughnesses (R_a/d_0) smaller than 2×10^{-3}. For larger surface roughnesses, the authors suggest additional investigations as insufficient data is available in the literature to establish reliable correlations.

In this paper, we examine the combined role of fluid dynamics and physical properties in the interaction of single drops with hot walls. This paper presents the results of drop-wall impact for single-component, bicomponent, and multicomponent liquid mixtures with a range of boiling points temperatures. The outcome of the drop-wall impact is characterized for a range of Weber number

(27–800) and wall temperatures (25–300 °C) spanning cold ambient wall conditions to high temperature wall conditions typical of combustor surfaces. The drop wall impact is characterized phenomenologically, and regime maps are presented for the single-component fuels. Subsequently, the impact of bicomponent drops consisting of n-heptane and n-decane are examined to characterize the role of the volatile component in the timescale and outcome of the drop-wall impact. Results are presented in regime diagrams, indicating the demarcation between different physical outcomes. Finally, the behaviors of typical multicomponent fuel drops are presented and compared with those of the bicomponent surrogate mixtures.

2. Experimental setup

This section presents details of the experimental setup and procedures and gives a description of image processing routines.

2.1. Drop generation and imaging setup

A schematic of the high-speed backlit imaging setup is shown in Fig. 1 consisting of the high speed camera, drop generator, and optics. A 1500-grit ground glass diffuser and a halogen lamp (500 W) were used for back illumination of the drops. A variable volume pipette (10–300 μL) was used to generate drops. The height of the pipette was changed to vary the impact velocity and corresponding Weber number. The pipette generated a single drop of approximately 1.8-mm diameter. During the drop impact, image sequences were recorded with a high-speed complementary metal-oxide-semiconductor camera (CMOS, Photron FASTCAM SA-X2). Images were obtained using a Nikon 105-mm focal length lens and 32 mm extension. The field of view and depth of field in these studies were 24×22 mm^2 and 22 mm, respectively. Images were captured at a rate of 20 kHz and with a shutter exposure of 48 μs, yielding a frame size of 1020×672 pixels^2. The imaging system results in a magnification of 19 μm per pixel. Images of the drop-wall impact were recorded from the side with the stage height set to the center of the frame.

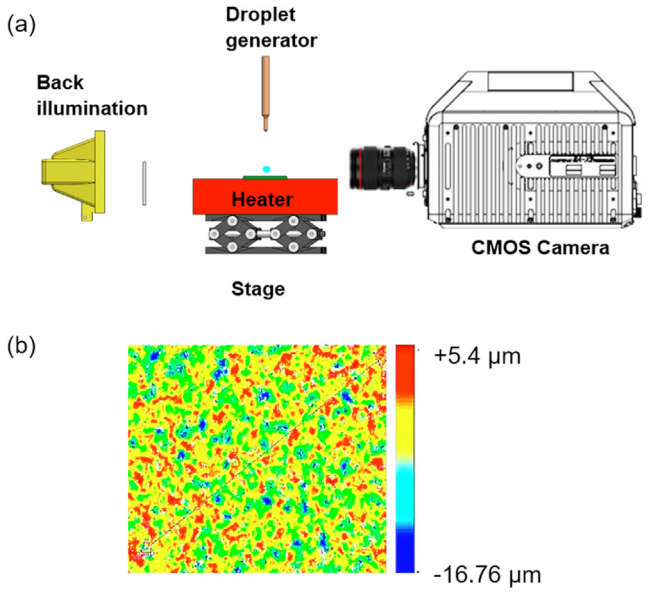

Fig. 1. (a) Schematic of high-speed backlit imaging setup used to record impact sequences at 20 kHz. (b) Interferometric surface profile measurement of the stainless-steel test surface.

After generation, the drop accelerated through ambient air onto a heated steel substrate (34×34 mm^2) held on a ceramic hot plate (171×171 mm^2) to obtain surface temperatures from 30 °C to 540 °C. The surface temperature was monitored for each test using a 3.175-mm K-type thermocouple with a tolerance of 2.2 °C (ASTM E230-ANSI). To ensure even heating of the test substrate, the surface temperature was measured at three different locations on the test substrate for each wall temperature set point. Thermocouples were in direct surface contact, and the locations consisted of the point of impact and two locations approximately 3 mm from the impact location. All image sequences were captured when the surface temperature had reached the desired steady-state value.

Stainless steel(SS 304) was used as a test substrate due to high resistance to thermal deformation. The surface roughness was controlled using blast media treatment. The roughness of the test surfaces was measured using an 3D optical surface profiler (Zygo, NewView 7100) and the roughness of the substrate surface is shown in Fig. 1(b). The measured R_z and R_a values for were 7.43 μm and 1.25 μm, respectively. R_z is the sum of the average peak values of tallest and lowest valleys from a mean line across the test substrate. R_a is the mean the amplitude across the measured line.

For the calculation of Weber numbers at impact, which will be used throughout the results, properties for the mixtures are estimated from the NIST REFPROP at a temperature of 21 °C [33]. Properties for the mixtures are calculated in REFPROP using data from Lemmon et al. and Rolo et al. [33,34].

2.2. Image processing

Image processing was implemented in MATLAB and used for measurement of the spread of the liquid film upon impact and the size of droplets resulting from secondary breakup. The image processing routine consisted of a normalization using a background image, followed by edge detection and measurement. In order to establish a consistent timebase across sequences, the time of impact was determined by tracking the centroid location relative to the surface. The time of impact is defined as the time when the centroid location of the drop reached a position equal to the drop radius. The drop velocity and diameter for each event were measured by identifying the centroid and extent in the 20 frames prior to impact. A Canny algorithm [35] is used to identify the edges of the drops and spread of the liquid film along the wall. Before applying the Canny algorithm, the image of the liquid film spread is background-subtracted, cropped, and dilated. After identifying the objects and edges in the image, the object with largest area is selected. The spread is defined as the total horizontal extent of the drop, as determined by this object.

A second routine was implemented in MATLAB to measure the secondary droplet number and size distribution after film breakup. The normalized image is subtracted from the background image, cropped, and filtered using a Gaussian kernel prior to edge detection (Fig. 2a, b). The Canny algorithm is applied after dilation to identify the edges of the secondary droplets (Fig. 2c). The centroid, major axis, minor axis, solidity, and effective diameter of the identified objects are measured for each detected object. In order to reliably detect single drops, the ratio of the major to minor axis is considered. Selecting objects with axes ratios of $d_{max}/d_{min} < 2$ in the routine ensures that the detected objects are approximately spherical and limits many of the overlapping droplets. Overlapping objects are challenging in image detection, so the reported droplet diameter distributions are made late in time, after the secondary drops have separated. The detected droplets are limited to sizes larger than approximately 50 μm. The system resolution was limited due to the necessity of capturing a relatively large field of view

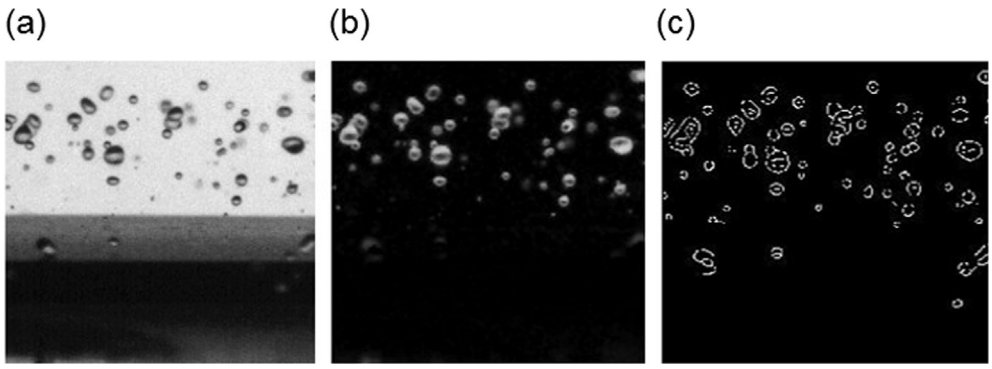

Fig. 2. Sample image processing sequence. (a) Raw image showing secondary breakup of n-heptane for $T_w = 300$ °C. (b) Background-subtracted and filtered image. (c) Edge detection result using a Canny algorithm.

and depth of field. As with all imaging experiments, identification of drops can suffer from several potential biases. These include the fairly to detect small drops due to image magnification or the inability to resolve these drops. In processing, we intentionally limited the smallest detectable size to 50 μm due to the system resolution. In addition, droplets in different planes may overlap, leading to undercounting or biases in the detected size. Finally, additional biases may exist if drops are non-spherical. Overall, these biases are relatively minor, but we limit the cases where sizes are measured directly to situations where the overall drop density is low enough so that shadowing is minor and drops are far from the wall.

2.3. Test parameters and sample information

Liquids included in these test consist of single-component representative hydrocarbons (n-heptane and n-decane) and bicomponent mixtures of these alkanes. Typical multicomponent fuels (gasoline, #2 diesel) have wide ranges of molecular weights and boiling points—potentially leading to complex behavior during impact with hot walls. As an example, the light and middle distillate fractions of a representative 91 AI gasoline consist mainly of alkanes [36]. The distillation curves of gasoline and diesel fuels used in the experiments are provided in the supplementary section. The distillation characteristics have been obtained using ASTM D86 test method [37]. The test consists of a 100 mL batch distillation at atmospheric pressure, during which the condensed volume is measured. The final result is expressed as percent recovered versus temperature.

In the studies presented, two alkanes were chosen which span the typical distillation fraction of gasoline. N-heptane serves as a low molecular weight/low-boiling point surrogate (at 20% of the distillation) with a boiling point of 98.5 °C. Furthermore, in modeling studies n-heptane is a well-accepted representative of gasoline [38,39]. N-Decane is a high boiling point alkane (174.5 °C) and is miscible with n-heptane, allowing a homogeneous binary mixture spanning a range of fuel-relevant boiling points. Binary mixtures were varied from 0 to 100% n-heptane by volume to allow study of the fuel composition effects on drop-wall impact. As previously described, wall temperatures are varied from 21 to 300 °C to span the nucleate boiling and film boiling regimes. These temperatures also span typically operating conditions in internal combustion engines. For example, piston crown temperatures of 300 °C have been reported for full load conditions [40,41].

3. Results

The outcome of experimental studies with fluids ranging from single-component to multicomponent fuels are compared for a range of impact Weber numbers on a dry heated wall. First, n-heptane is examined to establish distinct regimes as a function of wall temperature and the impact Weber number. Spread measurements with varying Weber number are presented, but these are limited to moderate wall temperatures before significant rebound and film boiling effects are evident. Using the regimes identified for single component drops, the role of the volatile component in a mixture of n-heptane and n-decane is examined. The size and number of secondary droplets generated for these cases are characterized for a range of mixtures. Finally, the impact of typical multicomponent fuels (gasoline and diesel) are discussed.

3.1. Impact of a pure single-component liquid (n-heptane)

The impact of single-component liquids with hot walls was extensively studied to characterize impact regimes, but some representative sequences are selected here for both varying wall temperature and varying impact velocity. Fig. 3 shows the outcomes for a range of wall temperatures (27, 100, 200, and 300 °C) for two conditions: low momentum impact with $We = 27$ and higher momentum impact with $We = 664$. Velocities of the n-heptane drops at impact are 0.8 ± 0.1 m/s, and 3.8 ± 0.2 m/s, respectively where the listed bounds reflect the experimental variation over a number of impact events.

A single drop-wall impact event is depicted in each horizontal row of frames in Fig. 3. For the $We = 27$ cases depicted in panel (a), the evolution is fairly slow and the time snapshots shown range from 2 ms after initial contact to 40 ms after initial contact. Examining the low-temperature case, at a wall temperature of 27 °C, the drop initially deposits as a liquid film on the wall surface and spreads to a maximum extent by 20 ms. As the wall temperature increases to 100 °C, near the saturation temperature of n-heptane (98.5 °C), the thin liquid film spreads to a maximum extent and then recoils slightly. After 40 ms, the liquid film undergoes nucleate boiling, as evident from the intense droplet ejections observed (not depicted).

Continuing to increase the wall temperature (T_w) results in total rebound of the drop at approximately 200 °C. This defines a Leidenfrost temperature for n-heptane of ~200 °C, consistent with the results of Chandra et al. [24] for n-heptane at a Weber number of 43. In the Fig. 3, the drop occasionally breaks up into a few fragments at $T_w = 200$ °C, but at significantly elevated wall temperatures ($T_w = 300$ °C), a complete rebound of the drop takes place with no additional breakup. Fig. 3(b) represents the outcomes for the same range of wall temperatures, but for an impact Weber number of 664. This impact velocity is moderate, so for cold wall conditions, no splashing is observed. However, increasing the wall temperature to the identified Leidenfrost temperature shows a significant change in behavior: first, splashing is observed at the edge

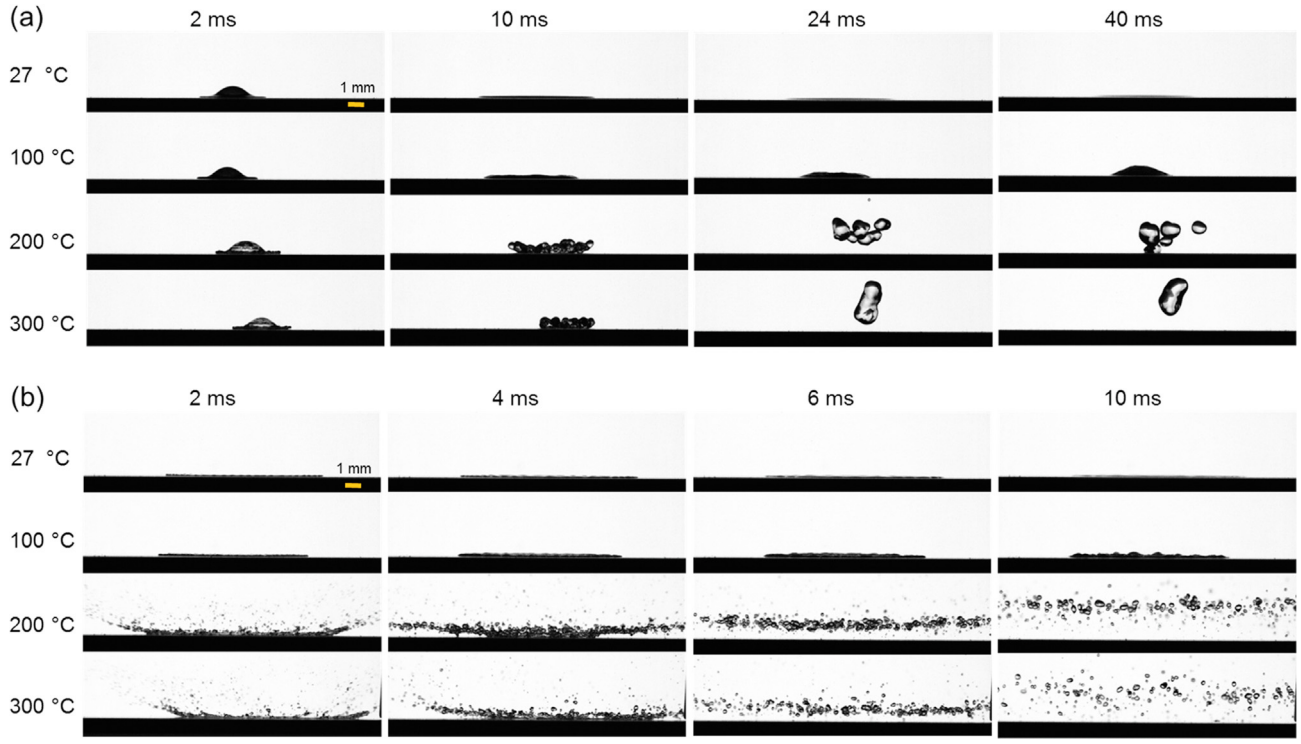

Fig. 3. Comparison of droplet impact sequences of n-heptane for (a) Weber number of 27 and (b) Weber number of 664 at wall temperatures ranging from ambient to above the Leidenfrost temperature.

of the spreading liquid film; second, the liquid film undergoes rapid breakup into a series of much smaller droplets which remain cushioned from the wall by vapor formation. Note that this occurs rapidly as compared to the sequences shown in Fig. 3(a), with splashing at the liquid film edge initiating prior to 2 ms and film breakup complete by 6 ms. Comparing the low and moderate *We* sequences at elevated wall temperature, increasing the impact momentum results in rapid spreading of the liquid film. At high wall temperatures, this results in vapor formation below a thin liquid film, and the subsequent film breakup occurs within a few milliseconds.

As exhibited in the sequences of Fig. 3(b), there are two characteristic formation mechanisms for secondary droplets during impact on a heated surface for n-heptane. Initially, secondary droplets are formed during a splashing event. These droplets are formed at the edge of the spreading liquid film, and can be termed corona splashing at the case shown: $We = 664$ at $T_w = 200$ and 300 °C, where prompt splashing has occurred prior to the frames shown at 2 ms in 3(b). The size of the secondary droplets formed due to prompt and corona splashing is notably smaller than those formed due to liquid film disintegration. Rioboo et al. also reported secondary droplet formation from splashing on dry cold walls at intermediate and high impact drop velocities [42]. For n-heptane, both prompt and corona splashing occur at wall temperatures well above the saturation temperature and at or above the Leidenfrost temperature (where rebound is observed for low-momentum drops).

After the initial splash, a liquid film spreads on the wall, but the higher momentum results in a thin liquid film (e.g. at 2 ms in Fig. 3 (b)). For higher wall temperatures, this liquid film begins to undergo breakup into secondary drops. At high wall temperatures, the film breakup occurs as rapid vapor formation at the liquid-wall interface results in a vapor cushion. Here, growth of instabilities can be considered as a shear layer instability with air on the upper liquid surface, and a thin vapor film on the lower surface. The growth of instabilities in free liquid sheets in air were examined first by Squire, who established a criterion for instability based on Weber number, $We > 1$, where the Weber number is defined by the relative velocity of the liquid film U and film height h as $We = \rho_l U^2 h/\sigma$ [43]. Clark, Dombrowski, and Taylor extended this analysis to the prediction of sinusoidal waves and showed good agreement in breakup lengths for conical and planar liquid sheets from spray nozzles [44]. Rangel and Sirignano analytically and computationally showed the existence of two distinct length scales related to dilational and sinous wave growth [45]. Here, the liquid film is spreading and the stability criteria established previously indicates a region of liquid film breakup [45]. During the breakup of the liquid film/sheet, the continuous formation of vapor near the hot wall results in the levitation of the liquid film. The mechanism of liquid film levitation on a hot substrate is explained by Roisman et al. [46]. After the drop impact, the outer part of the liquid levitates first as the liquid/vapor interface continues to expand away from the center of the liquid film. At this instant, most of the heat flux from the wall contributes towards evaporation of the liquid sheet. Bubbles grow, coalesce, and form a continuous layer of vapor between the liquid film and the hot wall [46,47]. This vapor flow separates the film into wetted and non-wetted (levitating) areas. Constant heat flux from the wall in the wetted area continuous to evaporate, developing a thermal boundary layer within the film. The liquid film/lamella detaches from the wall and levitates when the thermal boundary layer within the film reaches the free surface of the liquid film [46]. During the levitation of the liquid film, both sheet breakup and ligament breakup result in the formation of secondary droplets.

The results of n-heptane impacting on a dry, heated wall are summarized for a range of Weber number and wall temperature conditions in Fig. 4. The regime diagram shows a series of symbols along with a corresponding legend showing phenomenological classification. To summarize, first consider the behavior at low Weber number ($We < 100$). As described previously, at low wall

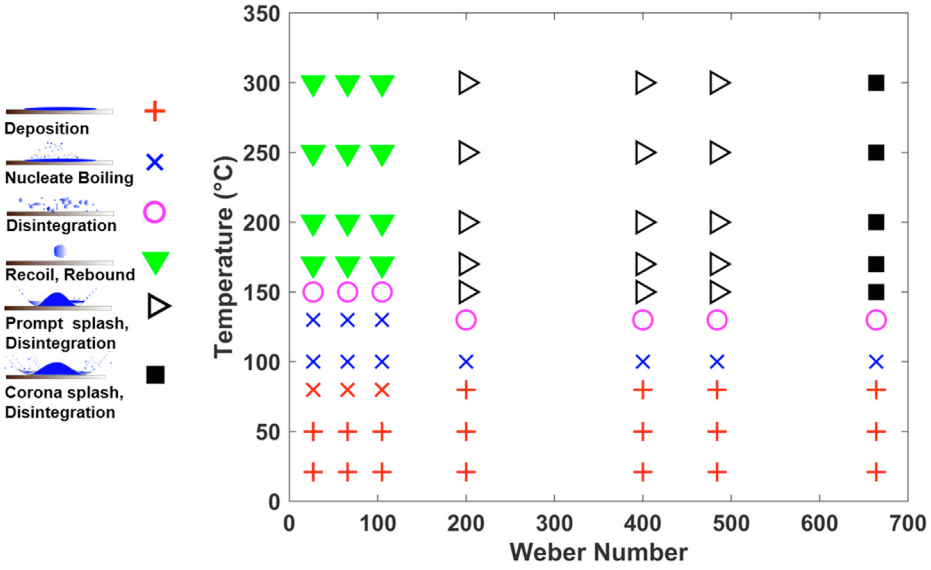

Fig. 4. The outcomes of n-heptane drops impacting a dry, heated wall are summarized for varying Weber number and wall temperature. At low temperature, the drops deposit on the wall without splashing. As the wall temperature increases, nucleate boiling and film breakup are observed. This is followed by rebound phenomena characterized by intact drop rebound at low We and prompt splashing and liquid film breakup at $We > 100$.

temperatures ($T_w < T_{sat}$), the drop contacts the wall and deposits, spreading into a thin liquid film. This liquid film has some maximum spread extent, and may ultimately recoil as the drop momentum dissipates through viscous losses at the wall and surface tension causes a return to a more spherical shape. As the wall temperature reaches and exceeds the saturation temperature ($T_w > T_{sat}$), the drop begins spreading on the wall, but significant bubble nucleation takes place and a fine cloud of droplets may be ejected from the liquid surface as these nucleation bubbles grow and collapse. Finally, at elevated wall temperature ($T_w > T_{Leidenfrost}$) for the low *We* case, there is rapid vapor formation near the wall, and the drop recoils and rebounds as a single drop from the wall. This is characterized as a Leidenfrost effect, and for consistency with much of the literature, we refer to a Leidenfrost temperature as the point where these low-velocity drops rebound, although the strict definition considers purely heat transfer rates for near-stationary drops.

For higher impact momentum ($We > 100$) several additional phenomena are observed. For the results presented for cold wall conditions, the outcome remains deposition up to the maximum of $We = 700$. As the work of Chandra et al. and Rioboo et al. has shown, continuing to increase *We* on cold walls leads to splashing [24,26]. For increasing wall temperature, similar nucleate boiling phenomena are observed for $T_{sat} < T_w < T_{Leidenfrost}$, where the Leidenfrost temperature is that of the near-stationary drop. Near the Leidenfrost temperature, the film tends to breakup (deemed disintegration), but there is still no evidence of splashing. Finally, for the highest wall temperatures, two distinct mechanisms for breakup of the primary drop are observed, as detailed previously. First, prompt splashing (or corona splashing) leads to small secondary drop production; and second, the liquid film disintegrates. The following sections will detail this disintegration behavior with attention to the role of the Leidenfrost temperature and the boiling point of the liquid. One additional note is the presence of a dynamic Leidenfrost temperature, previously explained by Yao et al. and Castanet et al. [48,49].

To examine the rate of spreading of the liquid film for n-heptane drops, a number of cases are shown in Fig. 5. Here, the spread factor (x/d_0) is determined from the maximum extent of the liquid feature measured following the edge detection proce-

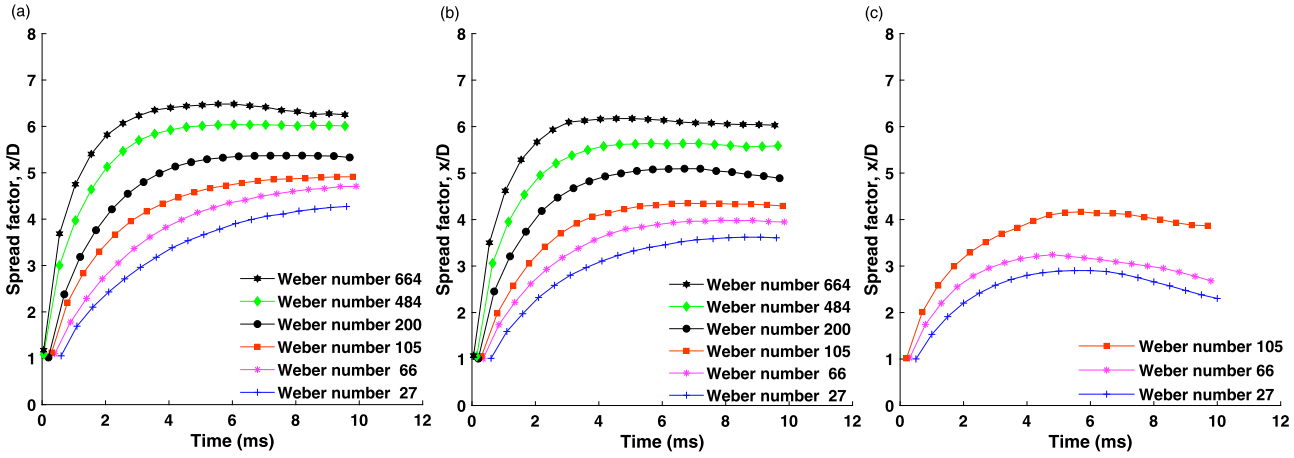

Fig. 5. Comparison of spread factor of n-heptane at Weber numbers of 27–664 at wall temperatures of (a) 27 °C and (b) 100 °C. (c) Comparison of spread factor of n-heptane at surface temperature of 150 °C and Weber numbers of 27–105.

dure outlined in the description of the experiment. Note that x is the distance between the two extreme ends of the liquid film spread. From left to right, the panels of Fig. 5 show the extent of spreading during impact normalized by the initial drop diameter for wall temperatures of 27 °C, 100 °C and 150 °C, respectively. Here, the increase in impact momentum is shown for representative impacts corresponding to Weber numbers of 27–664. For the highest wall temperature shown, 150 °C, the maximum *We* shown is limited to 105, as above this splashing takes place and the measurement of the spread of an intact liquid film is unclear. In each case, the extent of maximum spreading occurs earlier with higher *We*. From the time-resolved measurement, the maximum extent for a low $We = 27$ case occurs near 10 ms, while for $We = 664$, the maximum extent occurs around 4 ms. For wall temperatures of 27 and 100 °C, the recoil (decrease in maximum spread) is minimal over the 10 ms interval shown. These results indicate that predominant effects such as the spread of the liquid film are minimally impacted by changes in the liquid properties (e.g. liquid viscosity, surface tension). At elevated wall temperatures, approaching the point where Leidenfrost behavior is evident, the recoil of the drop becomes more prominent, and comparing 150 °C to 27 °C, the liquid film never reaches the maximum extent observed for the cold wall impact.

The spread factor for three different mixture compositions is shown in Fig. 6 at wall temperatures of 27 °C and 100 °C for the same moderate Weber number of ~484. In the film evaporation regime (T_w = 27 °C), the decrease in the concentration of n-heptane reduces the maximum spread. This moderate difference we attribute to the variation in surface tension of the liquid, as n-heptane has a reduced surface tension. At 20 °C, surface tension of n-decane is approximately 21% higher than n-heptane [34]. For elevated wall temperature (100 °C), the difference between mixtures is further reduced. As can be seen by comparing Figs. 5 and 6, the Weber number variation leads to much larger differences in the spreading rate and maximum spread than the mixture variation.

3.2. Impact of bicomponent drops (n-heptane and n-decane)

For bicomponent mixtures, the experimental results presented are focused on the aspects of the liquid film, rather than the onset of splashing. As a result, consideration of a range of *We* regimes gives a representative view. At low *We* (< 100), the results of the addition of a n-heptane to n-decane show little phenomenological difference with that of the pure n-decane. The predominant effects are the earlier onset of a Leidenfrost effect (rebound). As mentioned in the experimental discussion, the Weber numbers are estimated for ambient temperature conditions, and the mixture variation leads to a Weber number variation of 10% or less for the same impact velocity.

At moderate Weber number, the spreading of the liquid film results in additional unique behavior for a bicomponent mixtures. Considering the representative sequences in Fig. 7, a range of mixtures are shown spanning from pure n-decane to pure n-heptane, from left to right. The cases shown are at a wall temperature of 200 °C and $We = 484$. This wall temperature would be classified as below the Leidenfrost point for n-decane, but above the Leidenfrost point for n-heptane (200 °C). As a result, there is a transition between the two sets of phenomenological behaviors as the mixture concentration is varied from 0 to 100% n-heptane. For pure n-decane, the drop deposits, spreads as a thin liquid film, but exhibits no secondary drop formation either through splashing (prompt) or film breakup (delayed). With the addition of 30% n-heptane by volume, there is a distinct change in outcome: a small amount of splashing is evident, nucleate-boiling-like phenomena are observed by the small atomized drops at 3.7 ms, and a film breakup occurs in the liquid film by 10 ms, although the resulting droplets do not appear to be vapor-cushioned but stay attached to the wall. By increasing the more volatile n-heptane concentration to 50% and 60%, several phenomena become more prominent. First, splashing during initial impact is much more prevalent, promoted (as seen in pure components) by the formation of the vapor layer near the surface. Second, film breakup occurs within a few milliseconds. Third, increasing the volatile concentration increases the rebound height of the collection of drops after film breakup.

These results are summarized for a particular Weber number with varying wall temperature (T_w = 27–300 °C) and bicomponent concentrations (0–100% n-heptane) in the regime diagram of Fig. 8. At low wall temperature, deposition and spreading occurs for all bicomponent mixtures. As the wall temperature exceeds the boiling point of the volatile component (n-heptane), nucleate boiling is evident. For mixtures from 30 to 100% n-heptane, nucleate boiling phenomena are evident well below the n-decane saturation temperature. Increasing the wall temperature further promotes film breakup, but these outcomes again depend on the concentration. The higher concentration of n-heptane results in earlier film breakup, as well as increasing the distance of secondary drops upon rebound. The addition of the low-boiling point volatile compound at 30–70% leads to outcomes much closer to those of the pure n-heptane and effectively shifts vaporization-driven behavior. These outcomes indicate the importance of vapor formation effects in multicomponent fuels, even in cases where a significant volume fraction of fuel is well below the Leidenfrost temperature for significant fractions of the mixture (n-decane).

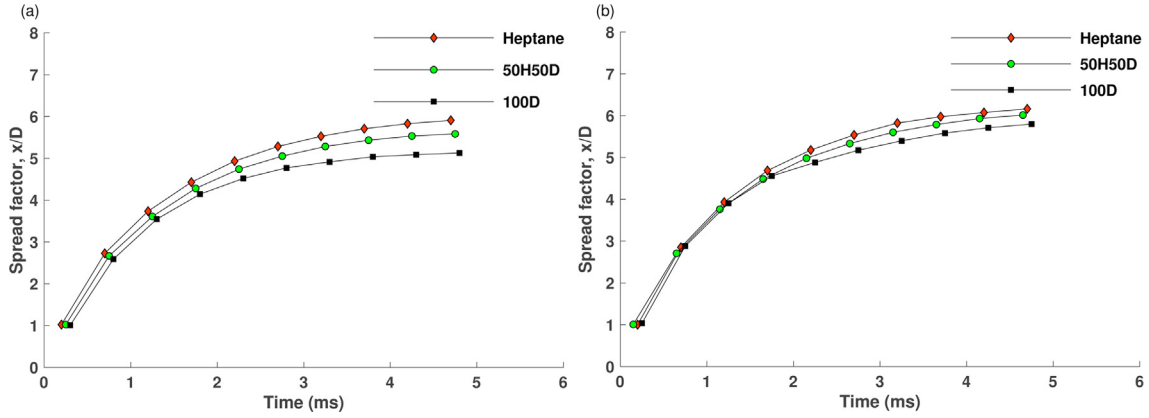

Fig. 6. Comparison of spread factor for n-heptane, a 50/50 mixture of n-heptane and n-decane, and n-decane is shown for a Weber number of 484 at wall temperatures of (a) 27 °C and (b) 100 °C.

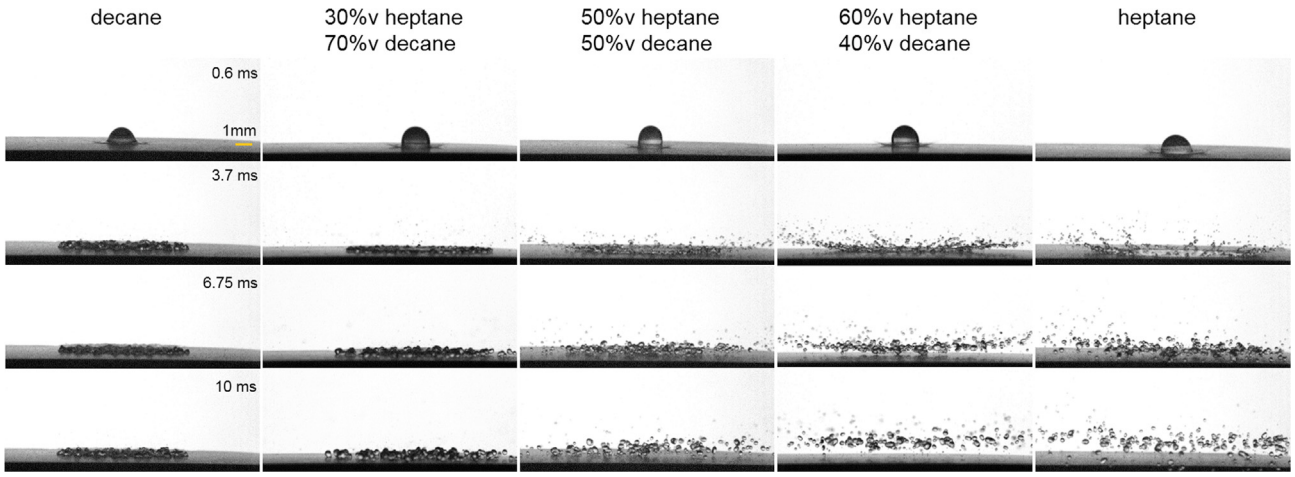

Fig. 7. Comparison of drop impact sequences of n-heptane, 60% v/v heptane, 50% v/v heptane, 30% v/v heptane, n-decane in the Weber number range of 425–484 and at surface temperature of 200 °C.

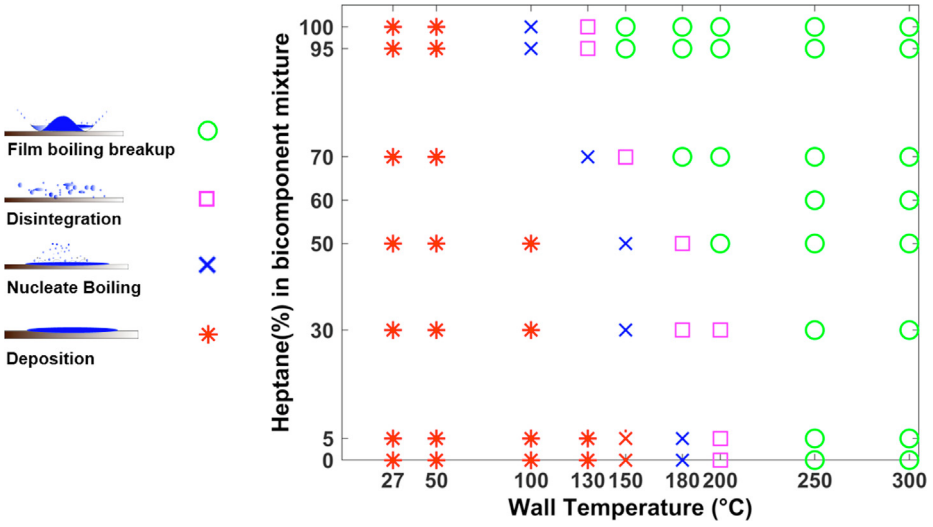

Fig. 8. Characterization of regimes for impact of bicomponent n-heptane/n-decane drops impacting walls for a moderate Weber number range of ($We = 425 - 484$) for wall temperatures ranging from 27 to 300 °C. Increasing the volatile concentration (n-heptane) results in a transition to a nucleate boiling and then liquid film disintegration at lower wall temperature relative to pure n-decane.

From the high-speed sequences of these bicomponent drop-wall impacts, the film breakup phenomena shows significant variation across mixtures. In order to evaluate the effect of mixture on the size and number of drops formed by film breakup, the Sauter mean diameter (d_{32}/d_0) is determined from image sequences. As introduced by Sauter [50,51], the Sauter mean diameter defines the diameter of a sphere with an equivalent volume-to-surface ratio as the droplet field:

$$d_{32} = \frac{\sum_{i=1}^{N} d_i^3}{\sum_{i=1}^{N} d_i^2} \tag{4}$$

Fig. 9 shows the Sauter mean diameter (d_{32}/d_0) normalized by the initial drop size for the two pure component fuels for a wall temperature of 300 °C and $We = 484$. The results presented are limited to high wall temperature cases where a direct comparison in secondary droplet sizes can be made for all bicomponent mixtures. At moderate temperatures (e.g. 200 °C, shown in Figs. 7 and 8) the regime shift is prominent, and in some cases no film breakup occurs. Taking this into consideration, the evolution of the normalized Sauter mean diameter for n-heptane and n-decane is shown in Fig. 9 for time instants from 4 to 15 ms after initial wall contact. Fig. 9 shows an increase in the normalized SMD ratio for both n-heptane and n-decane followed by a near-steady value by 15 ms. At each time-instant, the spread shows the range of measured normalized SMD over 10 independent sequences, with the 25–75% range shown as the filled bars and the mean indicated by the horizontal line. The late-time behavior shows a consistently higher normalized SMD of 0.17 for n-decane, compared to the 0.15 value for n-heptane.

At the late stage of film breakup, the drop size distribution is a function of the composition of the bicomponent mixtures. This is shown in Fig. 10 for a range of bicomponent mixtures, where the range of normalized Sauter mean diameter is shown at the time instant of 15 ms after the initial drop contact when the SMD reaches a quasi-steady state value. Here, the mean is indicated by the horizontal line, with the box representing the 25–75% range of normalized SMD for measurements from 10 independent events. As the amount of volatile component (n-heptane) decreases from 100% to 0%, d_{32}/d_0 increases. The addition of 5% n-decane to n-heptane has little influence on the Sauter mean diameter (SMD), but SMD increases by 10–12% when the volume fraction of n-

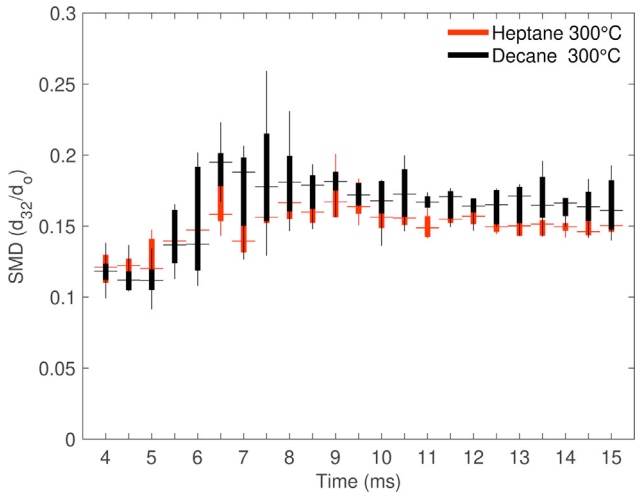

Fig. 9. Evolution of the normalized Sauter mean diameter of the secondary droplets for impact of n-heptane and n-decane at $We = 484$. Bars indicate the middle 50% and the mean over multiple events is indicated by the horizontal lines. Both fuels show a stationary distribution after approximately 10 ms.

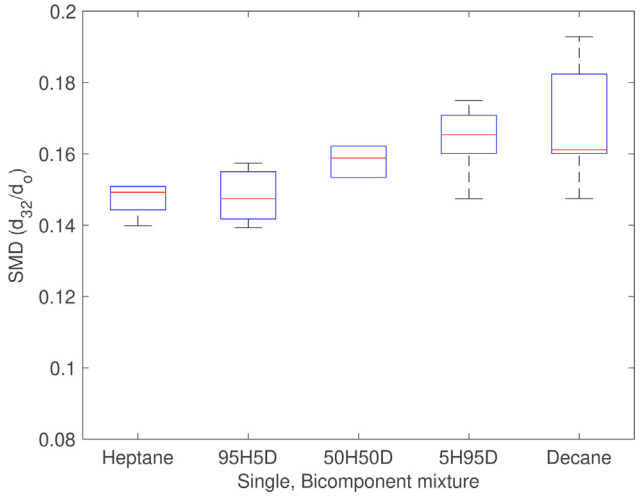

Fig. 10. Variation of the normalized Sauter mean diameter of the secondary droplets following impact on a hot wall ($T_w = 300$ °C, $We = 484$) at 15 ms.

decane is increased to 95%. This outcome implies that Sauter mean diameter of the secondary droplets is a function of low volatile component concentration in a bicomponent fuel mixture. As explained previously in Section 3.1, the mechanism of thin liquid film levitation and its disintegration into secondary droplets depend on the vaporization of the wetted area of the spreading liquid film. For bicomponent fuel mixtures with a higher percentage of low volatile component (n-decane in our case), the vaporization rate is lower and results in slower evolution of vapor layer between the hot wall and the thin liquid film. As vapor around the levitating liquid film plays an important role in the disintegration of the liquid sheet into secondary droplets, SMD for mixtures with a higher percentage of n-decane are higher.

3.3. Impact of multicomponent fuel drops (gasoline and diesel)

Following the characterization of bicomponent drop-wall impact, the behavior of two typical multicomponent commercial fuels were examined. Fig. 11 shows impact sequences for a commercial blend of gasoline fuel at Weber number of 484 for wall temperatures spanning from 21 to 300 °C. For typical gasoline blends, the 10–80% volume fraction distillation corresponds to boiling points from 65 to 175 °C [36]. The actual range of saturation temperature can vary based on location and the refinery source, but the composition of the fuel used in these studies is detailed in the Supplementary material. Examining the time sequences of gasoline drops impacting the dry wall indicates for general regimes, as was observed in the bicomponent mixtures. Between the wall temperature of 21 and 50 °C, a liquid film deposits and spreads, reaching a steady spreading extent after approximately 100 ms. Increasing the wall temperature between 100 and 150 °C shows a regime similar in qualitative appearance to nucleate boiling. Here, fine atomization takes place within a few milliseconds, but the liquid film remains for a significant duration (~100 ms). Further increase in the wall temperature begin to show vaporization-driven phenomena: prompt splashing and film breakup. From the representative sequence at 160 °C, prompt splashing and film breakup are evident, although drops from film breakup remain attached to the surface (characterized as a transition regime). The surface contact is shown explicitly by the presence of nucleation-induced atomization for this sequence. Increasing the temperature to 170 °C, the events are comparable to the film boiling ($T_w > T_{Leidenfrost}$) observed in single-component interactions and in bicomponent mixtures. With higher wall tem-

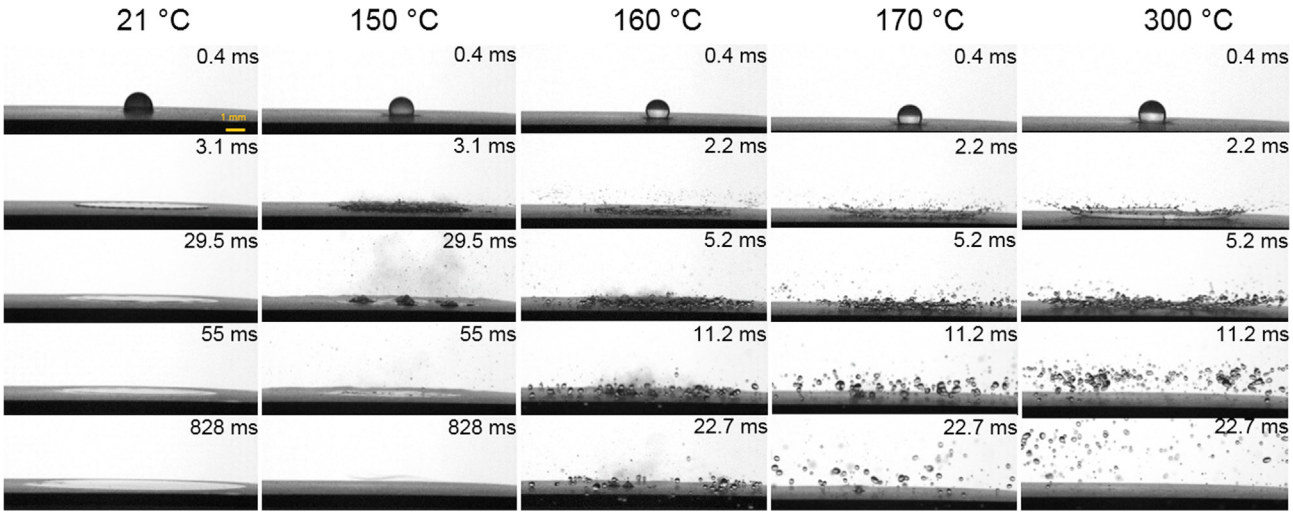

Fig. 11. Comparison of drop-wall impact sequences of gasoline fuel on for a Weber number of 484 and wall temperature range of 21–380 °C.

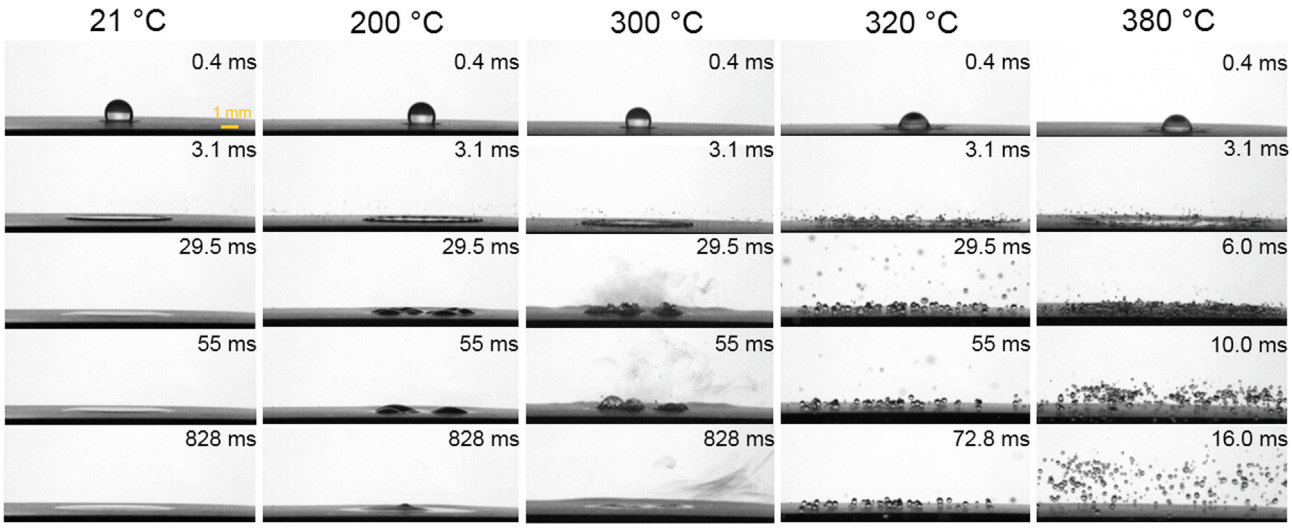

Fig. 12. Comparison of drop-wall impact sequences of diesel fuel on for a Weber number of 484 and wall temperature range of 21–380 °C.

perature, prompt splashing becomes more prominent, and secondary droplets formed from film breakup increase in velocity away from the wall.

Fig. 12 shows a representative set of sequences for the impact of diesel fuel drops at a comparable Weber number of 484 and for wall temperatures in the range of 21–380 °C. Diesel fuel blends have typical volume fraction distillations at higher distillation temperature than gasoline: 10–80% by volume corresponding to boiling points between 245 and 325 °C [52]. The impact sequences of diesel fuel can be similarly classified as film evaporation, nucleate boiling, transition, and film boiling regimes. Small-scale, prominent droplet ejections characterize the nucleate boiling regime at a wall temperature of 300 °C. Disintegration modes similar to those observed for bicomponent mixtures are present for wall temperatures of 320 and 380 °C, with significant drop contact with the wall evident at 320 °C. At the highest wall temperature ($T_w = 380$ °C), the vapor formation results in significant rebound velocities as vaporization effects dominate the secondary droplet motion. The wall temperatures for which these regimes are observed are consistently higher than those observed for gasoline, as expected due to the higher temperature distillation curve of typical diesel fuel blends. This is consistent to the offset in regime observed with increasing n-decane concentration in the bicomponent mixtures for a wall temperature of 200 °C and Weber number of 484 (Fig. 7). In general, the impact sequences for diesel drops take place on a longer timescales than gasoline–attributed to the comparable thermal transport timescales and higher saturation temperature of high molecular-weight components of diesel fuel.

4. Conclusions

In this paper, the role of liquid composition is characterized during the impact of the drops with hot walls. High-speed imaging sequences are used to characterize the regimes of drop-wall impact for single-component, bicomponent, and multicomponent liquid compositions relevant to combustors. For single component n-heptane drops, the onset of splashing and liquid film breakup are observed at elevated wall temperatures and Weber numbers approximately 200. The impact outcomes of bicomponent mixtures are also characterized for moderate Weber number. These results are used to generate a regime diagram with varying wall temperature and n-heptane concentration. The increase of the volatile liquid content is shown to promote rebound of drops and the promotion of liquid film disintegration at lower wall temperatures.

The regimes identified for bicomponent liquid mixtures are compared with the results for conventional multicomponent (commercial) liquid fuels, and the classified regimes are shown to be comparable to those identified for the well-defined bicomponent liquid mixtures. The experimental identification of regime boundaries and characterization of droplet sizes from prompt splashing and film breakup will enable validation of detailed spray-wall and drop-wall models essential for predicting the performance of combustion performance.

Declaration of Competing Interest

The authors declare no conflict of interest.

Acknowledgements

Support for this work was provided by the U.S. National Science Foundation (CBET-1332238, EPS-1101284).

Appendix A. Supplementary material

Supplementary data associated with this article can be found, in the online version, at https://doi.org/10.1016/j.ijheatmasstransfer.2019.06.033.

References

[1] M. Pais, L. Chow, E. Mahefkey, Surface roughness and its effects on the heat transfer mechanism in spray cooling, J. Heat Transf. 114 (1) (1992) 211–219.
[2] J. Yang, L. Chow, M. Pais, Nucleate boiling heat transfer in spray cooling, J. Heat Transf. 118 (3) (1996) 668–671.
[3] C.R. Ferguson, A.T. Kirkpatrick, Internal Combustion Engines: Applied Thermosciences, John Wiley & Sons, 2015.
[4] Q. Zhang, R.M. Ogren, S.-C. Kong, A comparative study of biodiesel engine performance optimization using enhanced hybrid pso–ga and basic ga, Appl. Energy 165 (2016) 676–684.
[5] M. Rein, Phenomena of liquid drop impact on solid and liquid surfaces, Fluid Dyn. Res. 12 (2) (1993) 61.
[6] Y. Li, S.-C. Kong, Coupling conjugate heat transfer with in-cylinder combustion modeling for engine simulation, Int. J. Heat Mass Transf. 54 (11–12) (2011) 2467–2478.
[7] K. Reif, Gasoline engine management, Bosch Professional Automotive Information, DOI 10 (2015), 978–3.

[8] A. Karl, A. Frohn, Experimental investigation of interaction processes between droplets and hot walls, Phys. Fluids 12 (4) (2000) 785–796.
[9] S.-C. Kong, Drop/Wall interaction criteria and their application in diesel spary modeling, Atomiz. Sprays 17 (6) (2007) 473–499, https://doi.org/10.1615/AtomizSpr.v17.i6.10.
[10] J. Breitenbach, J. Kissing, I.V. Roisman, C. Tropea, Characterization of secondary droplets during thermal atomization regime, Exp. Therm. Fluid Sci. 98 (2018) 516–522.
[11] C. Stow, M. Hadfield, An experimental investigation of fluid flow resulting from the impact of a water drop with an unyielding dry surface, Proc. R. Soc. Lond. A 373 (1755) (1981) 419–441.
[12] C. Mundo, M. Sommerfeld, C. Tropea, Droplet-wall collisions: experimental studies of the deformation and breakup process, Int. J. Multiph. Flow 21 (2) (1995) 151–173, https://doi.org/10.1016/0301-9322(94)00069-V.
[13] G.E. Cossali, M. Marengo, M. Santini, Thermally induced secondary drop atomisation by single drop impact onto heated surfaces, Int. J. Heat Fluid Flow 29 (1) (2008) 167–177, https://doi.org/10.1016/j.ijheatfluidflow.2007.09.006.
[14] R.L. Vander Wal, G.M. Berger, S.D. Mozes, The splash/non-splash boundary upon a dry surface and thin fluid film, Exp. Fluids 40 (1) (2006) 53–59.
[15] R. Li, N. Ashgriz, S. Chandra, Maximum spread of droplet on solid surface: low Reynolds and Weber numbers, J. Fluids Eng. 132 (6) (2010) 061302, https://doi.org/10.1115/1.4001695.
[16] T. Mao, D.C.S. Kuhn, H. Tran, Spread and rebound of liquid droplets upon impact on flat surfaces, AIChE J. 43 (9) (1997) 2169–2179, https://doi.org/10.1002/aic.690430903.
[17] Š. Šikalo, M. Marengo, C. Tropea, E.N. Ganić, Analysis of impact of droplets on horizontal surfaces, Exp. Therm. Fluid Sci. 25 (7) (2002) 503–510, https://doi.org/10.1016/S0894-1777(01)00109-1.
[18] G. Castanet, T. Liénart, F. Lemoine, Dynamics and temperature of droplets impacting onto a heated wall, Int. J. Heat Mass Transf. 52 (3–4) (2009) 670–679.
[19] V.E. Nakoryakov, S.Y. Misyura, S.L. Elistratov, The behavior of water droplets on the heated surface, Int. J. Heat Mass Transf. 55 (23–24) (2012) 6609–6617, https://doi.org/10.1016/j.ijheatmasstransfer.2012.06.069.
[20] G. Liang, I. Mudawar, Review of drop impact on heated walls, Int. J. Heat Mass Transf. 106 (2017) 103–126, https://doi.org/10.1016/j.ijheatmasstransfer.2016.10.031.
[21] V. Bertola, An impact regime map for water drops impacting on heated surfaces, Int. J. Heat Mass Transf. 85 (2015) 430–437.
[22] J.D. Naber, P.V. Farrell, Hydrodynamics of droplet impingement on a heated surface, SAE Trans. (1993) 1346–1361.
[23] A. Mills, J. Fry, Rate of evaporation of hydrocarbons from a hot surface: Nukiyama and Leidenfrost temperatures, Eur. J. Phys. 3 (3) (1982) 152.
[24] S. Chandra, C. Avedisian, On the collision of a droplet with a solid surface, Proc. R. Soc. Lond. A 432 (1884) (1991) 13–41.
[25] R. Rioboo, M. Marengo, C. Tropea, Time evolution of liquid drop impact onto solid, dry surfaces, Exp. Fluids 33 (1) (2002) 112–124, https://doi.org/10.1007/s00348-002-0431-x.
[26] R. Rioboo, C. Bauthier, J. Conti, M. Voué, J. De Coninck, Experimental investigation of splash and crown formation during single drop impact on wetted surfaces, Exp. Fluids 35 (6) (2003) 648–652, https://doi.org/10.1007/s00348-003-0719-5.
[27] E. Kompinsky, G. Dolan, E. Sher, Experimental study on the dynamics of binary fuel droplet impacts on a heated surface, Chem. Eng. Sci. 98 (2013) 186–194, https://doi.org/10.1016/j.ces.2013.04.047.
[28] A.-L. Biance, C. Clanet, D. Quéré, Leidenfrost drops, Phys. Fluids 15 (6) (2003) 1632–1637.
[29] M. Shirota, M.A.J. Van Limbeek, C. Sun, A. Prosperetti, D. Lohse, Dynamic Leidenfrost effect: relevant time and length scales, Phys. Rev. Lett. 116 (6) (2016) 1–5, https://doi.org/10.1103/PhysRevLett.116.064501, arXiv: 1511.04974.
[30] G.E. Cossali, M. Marengo, M. Santini, Secondary atomisation produced by single drop vertical impacts onto heated surfaces, Exp. Therm. Fluid Sci. 29 (8) (2005) 937–946, https://doi.org/10.1016/j.expthermflusci.2004.12.003.
[31] A. Moita, A. Moreira, Drop impacts onto cold and heated rigid surfaces: morphological comparisons, disintegration limits and secondary atomization, Int. J. Heat Fluid Flow 28 (4) (2007) 735–752.
[32] A.S. Moita, A.L. Moreira, Development of empirical correlations to predict the secondary droplet size of impacting droplets onto heated surfaces, Exp. Fluids 47 (4–5) (2009) 755.
[33] E.W. Lemmon, I. Bell, M.L. Huber, M.O. McLinden, NIST Standard Reference Database 23: Reference Fluid Thermodynamic and Transport Properties-REFPROP, Version 10.0, National Institute of Standards and Technology, 2018. https://doi.org/10.18434/T4JS3C. URL https://www.nist.gov/srd/refprop.
[34] L.I. Rolo, A.I. Caco, A.J. Queimada, I.M. Marrucho, J.A. Coutinho, Surface tension of heptane, decane, hexadecane, eicosane, and some of their binary mixtures, J. Chem. Eng. Data 47 (6) (2002) 1442–1445.
[35] J. Canny, A computational approach to edge detection, in: Readings in Computer Vision, Elsevier, 1987, pp. 184–203.
[36] B.L. Smith, T.J. Bruno, Improvements in the measurement of distillation curves. 3. Application to gasoline and gasoline+ methanol mixtures, Ind. Eng. Chem. Res. 46 (1) (2007) 297–309.
[37] A. International, D86-18 standard test method for distillation of petroleum products and liquid fuels at atmospheric pressure, in: ASTM Handbook, ASTM International, West Conshohocken, PA, 2018.
[38] L. Zhang, S.C. Kong, Vaporization modeling of petroleum-biofuel drops using a hybrid multi-component approach, Combust. Flame 157 (11) (2010) 2165–2174, https://doi.org/10.1016/j.combustflame.2010.05.011.
[39] L. Zhang, S.C. Kong, High-pressure vaporization modeling of multi-component petroleum-biofuel mixtures under engine conditions, Combust. Flame 158 (9) (2011) 1705–1717, https://doi.org/10.1016/j.combustflame.2011.01.002.
[40] E. Buyukkaya, M. Cerit, Thermal analysis of a ceramic coating diesel engine piston using 3-d finite element method, Surf. Coat. Technol. 202 (2) (2007) 398–402.
[41] S. Rahman, N. Fukamiya, M. Okano, K. Tagahara, K.-H. Lee, NII-electronic library service, Chem. Pharmaceut. Bull. 45 (9) (1997) 1527–1529, https://doi.org/10.1248/cpb.37.3229.
[42] R. Rioboo, C. Tropea, M. Marengo, Outcomes from a drop impact on solid surfaces, Atomiz. Sprays 11 (2) (2001) 12, https://doi.org/10.1615/AtomizSpr.v11.i2.40, arXiv: 1011.1669v3.
[43] H.B. Squire, Investigation of the instability of a moving liquid film, Br. J. Appl. Phys. 4 (6) (1953) 167–169, https://doi.org/10.1088/0508-3443/4/6/302.
[44] C.J. Clark, N. Dombrowski, Aerodynamic instability and disintegration of inviscid liquid sheets, Proc. Roy. Soc. A: Math. Phys. Eng. Sci. 329 (1579) (1972) 467–478, https://doi.org/10.1098/rspa.1972.0124, arXiv: 1108.0910.
[45] R.H. Rangel, W.A. Sirignano, The linear and nonlinear shear instability of a fluid sheet, Phys. Fluids A 3 (10) (1991) 2392–2400, https://doi.org/10.1063/1.858177.
[46] I. Roisman, J. Breitenbach, C. Tropea, Thermal atomisation of a liquid drop after impact onto a hot substrate, J. Fluid Mech. 842 (2018) 87–101.
[47] M.A. van Limbeek, M. Shirota, P. Sleutel, C. Sun, A. Prosperetti, D. Lohse, Vapour cooling of poorly conducting hot substrates increases the dynamic Leidenfrost temperature, Int. J. Heat Mass Transf. 97 (2016) 101–109.
[48] S.C. Yao, K.Y. Cai, The dynamics and Leidenfrost temperature of drops impacting on a hot surface at small angles, Exp. Therm. Fluid Sci. 1 (4) (1988) 363–371, https://doi.org/10.1016/0894-1777(88)90016-7.
[49] G. Castanet, O. Caballina, F. Lemoine, Drop spreading at the impact in the Leidenfrost boiling, Phys. Fluids 27 (6) (2015) 063302.
[50] J. Sauter, Die Grössenbestimmung der im Gemischnebel von Verbrennungskraftmaschinen vohrhandenen Brennstoffteilchen:(Mitteilung aus dem Laboratorium für Technische Physik der Technischen Hochschule München), VDI-Verlag, 1926.
[51] A.H. Lefebvre, V.G. McDonell, Atomization and Sprays, CRC Press, 2017.
[52] B.L. Smith, L.S. Ott, T.J. Bruno, Composition-explicit distillation curves of diesel fuel with glycol ether and glycol ester oxygenates: fuel analysis metrology to enable decreased particulate emissions, Environ. Sci. Technol. 42 (20) (2008) 7682–7689.